JCI The Journal of Clinical Investigation

Cerebral amyloid-β proteostasis is regulated by the membrane transport protein ABCC1 in mice

Markus Krohn, … , Lary C. Walker, Jens Pahnke

J Clin Invest. 2011;121(10):3924-3931. https://doi.org/10.1172/JCI57867.

Research Article **Neuroscience**

In Alzheimer disease (AD), the intracerebral accumulation of amyloid-β (Aβ) peptides is a critical yet poorly understood process. Aβ clearance via the blood-brain barrier is reduced by approximately 30% in AD patients, but the underlying mechanisms remain elusive. ABC transporters have been implicated in the regulation of Aβ levels in the brain. Using a mouse model of AD in which the animals were further genetically modified to lack specific ABC transporters, here we have shown that the transporter ABCC1 has an important role in cerebral Aβ clearance and accumulation. Deficiency of ABCC1 substantially increased cerebral Aβ levels without altering the expression of most enzymes that would favor the production of Aβ from the Aβ precursor protein. In contrast, activation of ABCC1 using thiethylperazine (a drug approved by the FDA to relieve nausea and vomiting) markedly reduced Aβ load in a mouse model of AD expressing ABCC1 but not in such mice lacking ABCC1. Thus, by altering the temporal aggregation profile of Aβ, pharmacological activation of ABC transporters could impede the neurodegenerative cascade that culminates in the dementia of AD.

Cerebral amyloid-β proteostasis is regulated by the membrane transport protein ABCC1 in mice

Markus Krohn,[1,2] Cathleen Lange,[1,2] Jacqueline Hofrichter,[1,2] Katja Scheffler,[1,2] Jan Stenzel,[1,2] Johannes Steffen,[1] Toni Schumacher,[1] Thomas Brüning,[1] Anne-Sophie Plath,[1,3] Franziska Alfen,[1] Anke Schmidt,[1,3] Felix Winter,[1,2,4] Katja Rateitschak,[4] Andreas Wree,[5] Jörg Gsponer,[6] Lary C. Walker,[7] and Jens Pahnke[1,2,3]

[1]Department of Neurology, Neurodegeneration Research Laboratory (NRL), [2]Interdisciplinary Faculty, Department of Aging Science and Humanities, [3]German Centre for Neurodegenerative Diseases (DZNE), Rostock Centre, [4]Institute of Systems Biology and Bioinformatics, and [5]Institute of Anatomy, University of Rostock, Rostock, Germany. [6]Center for High-Throughput Biology, University of British Columbia, British Columbia, Vancouver, Canada. [7]Yerkes National Primate Research Center and Department of Neurology, Emory University, Atlanta, Georgia, USA.

In Alzheimer disease (AD), the intracerebral accumulation of amyloid-β (Aβ) peptides is a critical yet poorly understood process. Aβ clearance via the blood-brain barrier is reduced by approximately 30% in AD patients, but the underlying mechanisms remain elusive. ABC transporters have been implicated in the regulation of Aβ levels in the brain. Using a mouse model of AD in which the animals were further genetically modified to lack specific ABC transporters, here we have shown that the transporter ABCC1 has an important role in cerebral Aβ clearance and accumulation. Deficiency of ABCC1 substantially increased cerebral Aβ levels without altering the expression of most enzymes that would favor the production of Aβ from the Aβ precursor protein. In contrast, activation of ABCC1 using thiethylperazine (a drug approved by the FDA to relieve nausea and vomiting) markedly reduced Aβ load in a mouse model of AD expressing ABCC1 but not in such mice lacking ABCC1. Thus, by altering the temporal aggregation profile of Aβ, pharmacological activation of ABC transporters could impede the neurodegenerative cascade that culminates in the dementia of AD.

Introduction

Proteostasis is achieved in cells and tissues by interactive mechanisms that regulate the production, folding, localization, binding, and disposal of proteins (1). In patients with Alzheimer disease (AD), a disequilibrium of proteostasis in the brain leads to the accumulation of oligomeric and fibrillar multimers of the peptide amyloid-β (Aβ) (1–3). Aβ clearance from the brain is reduced by approximately 30% in AD patients compared with healthy controls (4). The principal known mechanisms that contribute to the elimination of Aβ are degradation (by enzymes, the proteasome complex, and autophagy) (5, 6), active, receptor-mediated transcytotic transport across the blood-brain barrier by LRP1 and RAGE, and by perivascular drainage of the extracellular fluid (7–11). In addition, 3 members of the ATP-binding cassette transporter family — ABCA1, ABCB1, and ABCG2 — have been shown to export Aβ (12–18). Members of different ABC transporter subfamilies exhibit different export kinetics for specified substrates (19, 20). However, the role of the subfamily C of ABC transporters in the export of Aβ has not yet been investigated. To address this question, we compared the ability of specific ABC transporters (ABCB1, ABCG2, and ABCC1) to clear Aβ in vitro and in genetically modified mice. We found that the transporter ABCC1 strongly influences Aβ transport and accumulation in vivo, and thus represents what we believe is a novel target for regulating Aβ proteostasis in the brain.

Authorship note: Markus Krohn and Cathleen Lange contributed equally to this work.

Conflict of interest: The authors have declared that no conflict of interest exists.

Citation for this article: *J Clin Invest.* 2011;121(10):3924–3931. doi:10.1172/JCI57867.

Results

Increased Aβ burden in ABCB1- and ABCC1-deficient mice. We established new mouse models that express Swedish mutant human Aβ precursor protein (APPswe) and mutant presenilin-1 (PS1) (hereafter referred to as *APP/PS1*) that lack specific ABC transporters — ABCC1 (*Abcc1*$^{-/-}$), ABCB1 (*Abcb1*$^{-/-}$), and ABCG2 (*Abcg2*$^{-/-}$) (see Methods). Using Aβ immunohistochemistry, we found highly significant increases in the cortical load and size of Aβ-positive plaques in *APP/PS1*×*Abcc1*$^{-/-}$ mice as compared with *APP/PS1* mice. *APP/PS1*×*Abcb1*$^{-/-}$ mice showed a smaller increase in Aβ lesions, but no consistent difference was observed between *APP/PS1* controls and *APP/PS1*×*Abcg2*$^{-/-}$ mice (Figure 1 and Supplemental Figure 1, A–D; supplemental material available online with this article; doi:10.1172/JCI57867DS1). Because of variations in the molecular packing density of Aβ in senile plaques, histological assessment of plaques can only yield an approximate estimate of the total amount of aggregated Aβ in the brain (21). Thus, we also employed ELISAs for Aβ40 and Aβ42 to determine the total amount of buffer-soluble Aβ (mostly monomers and small oligomers) and guanidine-soluble Aβ (mostly fibrillar material) in the brain. *APP/PS1*×*Abcc1*$^{-/-}$ mice showed a significant increase in aggregated (guanidine-soluble) Aβ42 and Aβ40 as compared with *APP/PS1* control mice at all time points measured (Supplemental Figure 2A and Supplemental Figure 3A). At 25 weeks of age (the oldest age studied), guanidine-soluble Aβ40 and Aβ42 levels were 14-fold and 12-fold greater, respectively, in *APP/PS1*×*Abcc1*$^{-/-}$ mice than in control mice (Figure 2A, Supplemental Figure 2A, and Supplemental Figure 3A). Buffer-soluble Aβ40 and Aβ42 also increased with age (Supplemental Figure 2B and Supplemental Figure 3B), but at week 25 (when plaque load was highest), buf-

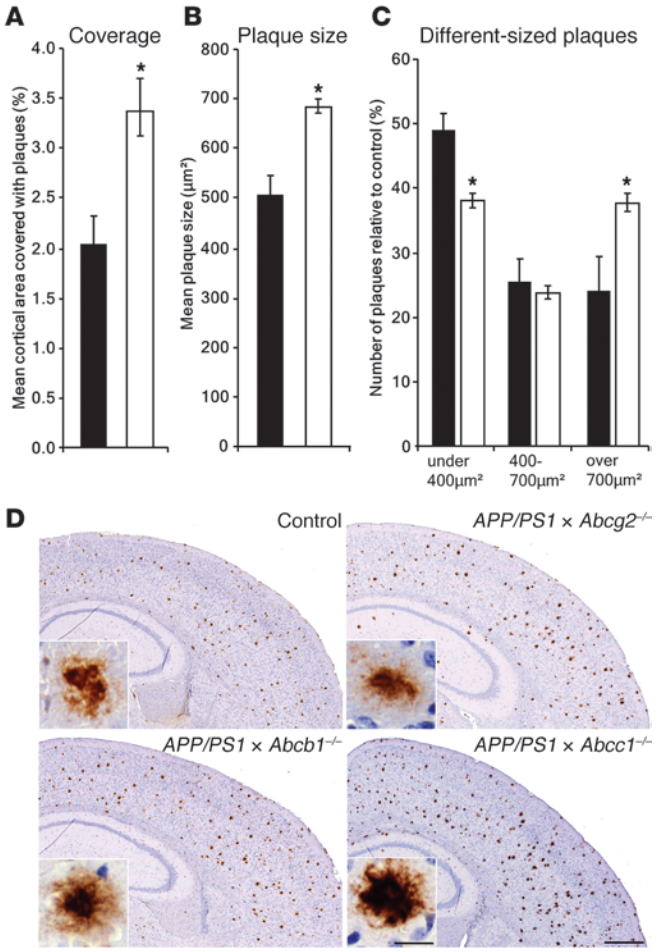

Figure 1
ABCC1 deficiency promotes Aβ deposition. (**A**) Cortical areal density of Aβ plaques is elevated by approximately 75% in *APP/PS1×Abcc1*$^{-/-}$ (controls, black bars; *APP/PS1×Abcc1*$^{-/-}$, white bars). (**B** and **C**) Mean plaque size is increased (+34%) due to the greater number of plaques (+63%) larger than 700 μm² and a lower frequency of small plaques (–24%). Error bars show SEM. *$P < 0.05$. $n \geq 3$. (**D**) Immunohistochemical stains of *APP/PS1×Abcg2*$^{-/-}$, *APP/PS1×Abcb1*$^{-/-}$, *APP/PS1×Abcc1*$^{-/-}$, and control mice reveal the greater areal density of Aβ in *Abcc1*$^{-/-}$ animals. Typical plaques of similar size are depicted in the insets. Scale bars: 500 μm (insets, 50 μm). Age of animals, 25 weeks.

fer-soluble Aβ42 levels declined precipitously in the *Abcc1*$^{-/-}$ group (Figure 2B). The exaggerated group differences in Aβ burden measured by ELISA compared with the smaller differences found in morphological quantifications may be due to the aggressive nature of the mouse model used. It has been shown earlier that cortical plaque coverage in these mice increases almost linearly, whereas total Aβ accumulation measured by ELISA increases exponentially with age due to higher Aβ packing density (i.e., histology is an areal measurement, whereas ELISA is essentially a volumetric measurement) (22). Hence, ELISA yields a more accurate assessment of total cerebral Aβ load in this model.

APP shedding, processing, and degradation. To control for changes in APP processing enzymes and Aβ transcytosis, which may influence Aβ load in *APP/PS1×Abcc1*$^{-/-}$ mice, we assessed the levels of APP-shedding enzymes/Aβ-proteases, and Aβ membrane receptors using mRNA gene chip and protein analyses. ADAM10 protein expression was increased in *APP/PS1×Abcc1*$^{-/-}$ mice, while the expression of the other analyzed enzymes (APP full length, APH1a-c, BACE1, BACE2, ECE1, ECE2, IDE, LRP1, NEP, NCST, PEN2, PS1, PS2, RAGE) was unchanged (Supplemental Figure 4 and Supplemental Table 5).

Another potential influence on Aβ load is microglial activation, which affects plaque size and may contribute to early Aβ degradation (23). Since *Abcc1*$^{-/-}$ mice are known to have a diminished inflammatory response (24), we sought to rule out a role of reduced microglial activity in the augmentation of Aβ pathology. Double immunostaining for microglia using antibodies to Iba1 and Aβ (23) revealed markedly increased plaque-associated microglia at age 25 weeks in all transporter-deficient strains, with the greatest microgliosis in *APP/PS1×Abcc1*$^{-/-}$ mice (Supplemental Figure 5), reflecting the increased amyloid burden in these mice and indicating that the exaggerated Aβ burden in this model does not result from a paucity of microglia.

ABCC1 facilitates Aβ transport in vitro. To further assess the role of ABCC1 in Aβ clearance, we compared the ability of *Abcc1*$^{-/-}$ and WT endothelia to transport Aβ42 in vitro in endothelial cell Transwell assays (ECTAs) of primary cultured capillary endothelial cells from mouse brains. The deficiency of ABCC1 reduced Aβ42 transport by approximately 60% in this in vitro model (Figure 2C).

Mathematical simulation and prediction of Aβ clearance kinetics. Next, we wanted to establish whether a single mathematical model that describes the basic physiological processes contributing to the production and removal of Aβ aggregates can capture the kinetics of different Aβ species in the *APP/PS1×Abcc1*$^{-/-}$ mice. Most importantly, we asked whether such a model would highlight the key role of Aβ transport and whether it would have predictive power for other mouse strains. The model that we developed does not describe detailed mechanisms, but rather captures the inclusive effect of all essential players in Aβ proteostasis, including transport proteins that are involved in Aβ influx/efflux (Figures 3 and 4, Supplemental Methods/Equations, and Supplemental Tables 1–3). Although parameter values of the model were estimated only from concentration time series of buffer-soluble Aβ42 in *APP/PS1×Abcc1*$^{-/-}$ mice (Figure 4A), the model accurately predicts the temporal aggregation profile for guanidine-soluble Aβ42 concentrations as well (Figure 4B). Importantly, when the simulated rate for Aβ clearance is increased by approximately 11% compared with *APP/PS1×Abcc1*$^{-/-}$ mice, the model predicts slower aggregation profiles that are nearly identical to those we observed in *APP/PS1×Abcb1*$^{-/-}$ mice (Figure 4, C and D). This model thus captures the principal mechanisms underlying the aggregation and transport of Aβ42 in *APP/PS1×Abcc1*$^{-/-}$ mice and underscores the importance of ABC transporters for Aβ proteostasis.

$Aβ_{dt}$ is extensively cleared by ABCC1. The *APP/PS1* mouse is an aggressive model of cerebral Aβ proteopathy in which even minor alterations may lead to large changes in Aβ accumulation. Therefore, we sought to analyze a mouse model of β-amyloidosis that develops deposits more slowly. Notably, the clearance kinetics of ABC transporters also are dependent on specific peptide characteristics, such as charge (9, 20). The Dutch-type mutation (Glu693Gln in hAPP770) of APP (*APP_{dt}*), which alters the charge near the α-secretase cleavage site of APP and causes severe cerebral

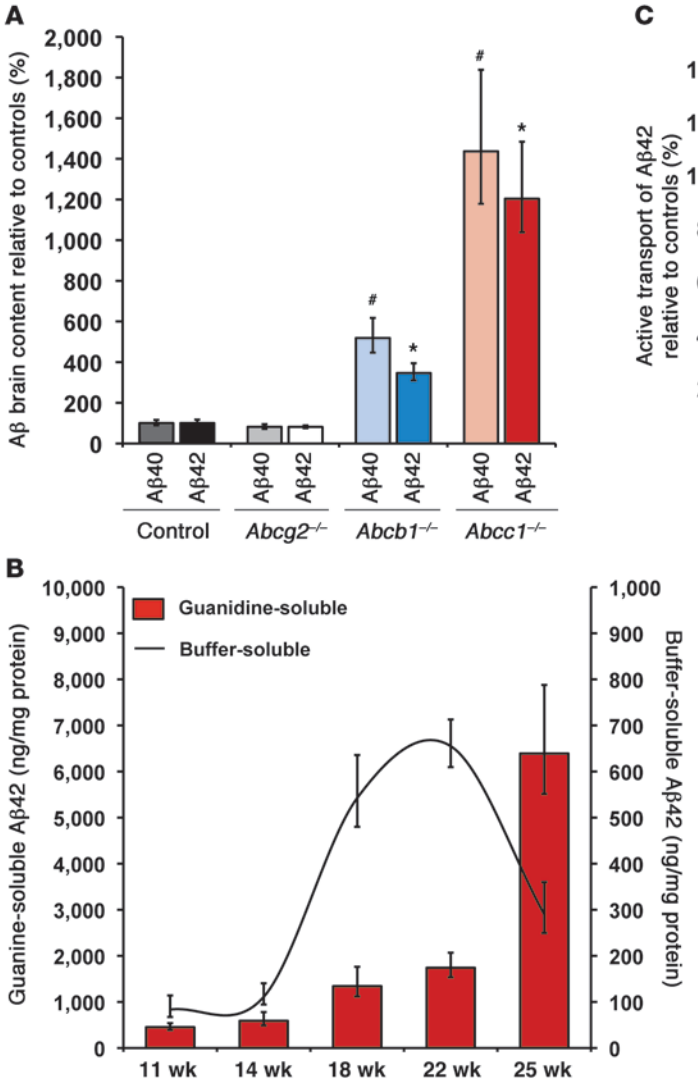

Figure 2
Deficiency of ABCC1 promotes the accumulation of Aβ. (**A**) At age 25 weeks, ABCC1 deficiency leads to a marked increase in insoluble Aβ as measured by ELISA. $n \geq 4$. $^{\#}P < 0.05$ versus Aβ40; $^{*}P < 0.05$ versus Aβ42. (**B**) Buffer-soluble Aβ42 is precipitously reduced at age 25 weeks versus 22 weeks (–56%), possibly due to its deposition into insoluble deposits within the brain. At this same age, the area occupied by Aβ deposits measured by immunohistochemistry is elevated by 83% (Supplemental Figure 1). Error bars show SEM. $n \geq 5$. (**C**) Transport of Aβ42 from the abluminal (brain) into the luminal (blood) compartment is impaired in *Abcc1*$^{-/-}$ endothelia. The mean Aβ42 transport rate of *Abcc1*$^{-/-}$ cells during the first 6 hours after addition of Aβ42 peptides was only 40% of control cells. Error bars show SEM. $n = 3$.

amyloid angiopathy (CAA) (25), has been shown to impair the elimination of $A\beta_{dt}$ via the blood-brain barrier (26). We hypothesized that *APP*$_{dt}$-transgenic mice that are deficient in ABC transporters will have altered accumulation of $A\beta_{dt}$ along the perivascular drainage channels (8). To test this hypothesis, we crossed *Abcc1*$^{-/-}$, *Abcb1*$^{-/-}$, and *Abcg2*$^{-/-}$ mice with *APP*$_{dt}$ mice. Because *APP*$_{dt}$ mice normally begin to manifest CAA around 22 months of age, we quantified the degree of CAA in the *APP*$_{dt}$×*ABC*-deficient mice at 24 months of age. Both the number and severity of Aβ-immunoreactive vessels were significantly increased in *APP*$_{dt}$×*Abcc1*$^{-/-}$ animals compared with *APP*$_{dt}$ controls, but not in *APP*$_{dt}$×*Abcg2*$^{-/-}$ or in *APP*$_{dt}$×*Abcb1*$^{-/-}$ mice (Figure 5, see Supplemental Figure 9 for exemplary pictures). Furthermore, we found serum leakage but no microhemorrhages in *APP*$_{dt}$×*Abcc1*$^{-/-}$ mice (data not shown). In addition to CAA, Aβ was increased in neurons of the neocortex (layer 5) and hippocampus of *APP*$_{dt}$×*Abcc1*$^{-/-}$ mice. Immunohistochemical staining suggested that the immunoreactive structures were vesicular in nature (Supplemental Figure 6, C and D), and subcellular fractionation confirmed that Aβ immunoreactivity resided mainly within the calreticulin-positive microsomal compartment (Supplemental Figure 6, A and B).

Activation of ABCC1 reduces Aβ burden. An important implication of our findings is that the drug-mediated activation of specific ABC transporters should reduce soluble Aβ levels in the brain. To test this hypothesis, we searched for an ABCC1 activator currently in clinical use. Because ABC transporters are the main contributors to chemoresistance in cancer cells, the principal therapeutic objective has been the development of inhibitors, but we identified one drug, thiethylperazine, that activates ABCC1 transport activity in vitro by 69% (Supplemental Figure 7 and ref. 27). Unfortunately, thiethylperazine also inhibits the function of ABCB1 (27). With this caveat in mind, we initiated a prevention paradigm in which we treated young *APP/PS1* and *APP/PS1*×*Abcc1*$^{-/-}$ mice (here, the negative control) for 30 days with thiethylperazine twice daily at 3 mg/kg body weight (i.m., human-adapted dose) starting at 45 days of age. This age precedes the normal appearance of senile plaques in this model (22, 23). ELISA measurements revealed that thiethylperazine significantly reduced Aβ42 levels in *APP/PS1* mice, but not in the *APP/PS1*×*Abcc1*$^{-/-}$ mice (Figure 6, A and B).

To date, idiopathic AD is not predictable in humans and diagnosis is made after disease onset. Therefore, we also tested a post-onset treatment paradigm in which mice were given a human-

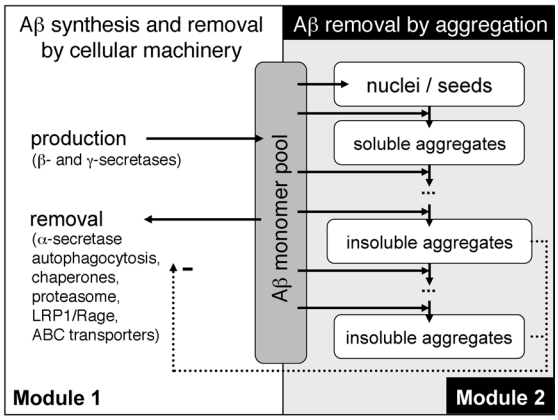

Figure 3
Schematic representation of the mathematical model. The mathematical model consists of 2 modules. Module 1, production of monomeric Aβ and its removal from the Aβ monomer pool. Production occurs at a constant rate, while removal of monomeric Aβ by active ABC transporters is influenced by the abundance of insoluble Aβ aggregates. Module 2, nucleation of monomeric Aβ and growth of the nuclei by addition of Aβ monomers. Both modules share the same pool of monomeric Aβ and interact via the impeding influence of insoluble aggregates considered in module 2 on the activity of the transport mechanism considered in module 1. Equations of the mathematical model are restricted to 3 basic mechanisms: (a) regulation of monomer abundance via production and removal; (b) nucleation; and (c) irreversible growth by monomer addition.

adapted dose of 15 mg thiethylperazine per kg body weight (p.o.) from age 75 days to 100 days. Per oral treatment was chosen in this paradigm to mimic the route of application most feasible for patients. Treatment of *APP/PS1* mice resulted in a significant 65% decrease of buffer-soluble Aβ (Figure 6D and Supplemental Figure 8B). Although reduction of guanidine-soluble Aβ content did not reach significance, the number of plaques and mean plaque size were reduced by 52% and 40%, respectively (Figure 6, C, E, and F, and Supplemental Figure 8A). To control for the inhibiting effect of thiethylperazine on ABCB1, we also treated *Abcb1*$^{-/-}$ mice. Consistent with the role of ABCB1 in Aβ clearance, the effect of thiethylperazine treatment was augmented in *Abcb1*$^{-/-}$ mice, as both the buffer-soluble and guanidine-soluble Aβ40 and Aβ42 were decreased significantly (Supplemental Figure 8, C–F). Thus, thiethylperazine administration supports the conclusion that ABCC1 is an important Aβ exporter and suggests that selective activation of ABCC1 is a potentially promising therapeutic objective for AD treatment or prevention.

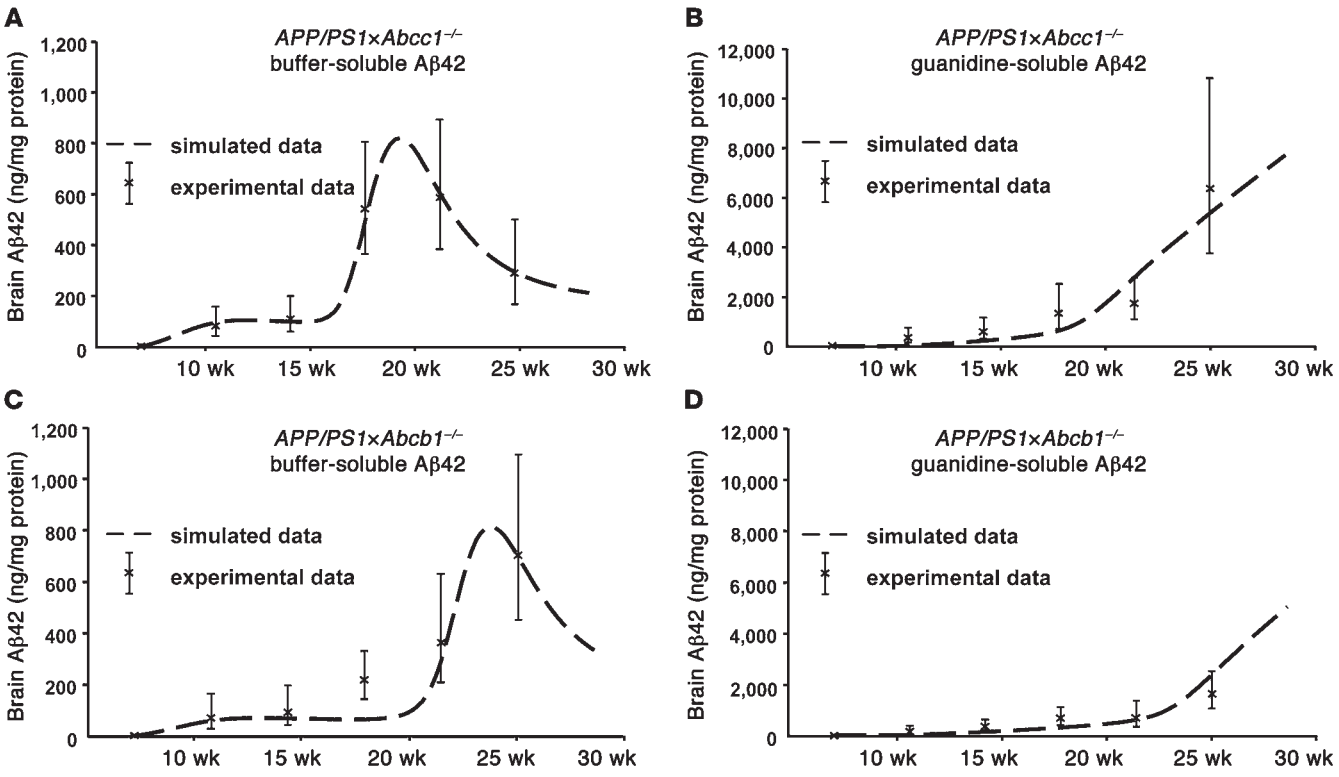

Figure 4
Simulation and prediction of Aβ proteostasis regulated by ABC transporters. (**A** and **B**) Temporal profile of Aβ42 aggregation as predicted by the mathematical model mapped to Aβ42 ELISA measurements of *APP/PS1×Abcc1*$^{-/-}$ mouse brains (**A**, soluble pool; **B**, insoluble pool). Although parameter value estimation focused on the soluble aggregates only, our model also correctly predicts the aggregation profile for insoluble Aβ42. (**C** and **D**) Temporal profile of Aβ42 aggregation as predicted by the mathematical model with an 11% increase of transport capacity (compared with the optimized parameter set for *APP/PS1×Abcc1*$^{-/-}$ mice) mapped to Aβ42 ELISA measurements of *APP/PS1×Abcb1*$^{-/-}$ mouse brains (**C**, soluble pool; **D**, insoluble pool). The increase in transport capacity results in a temporal aggregation profile as seen in *APP/PS1×Abcb1*$^{-/-}$ mice.

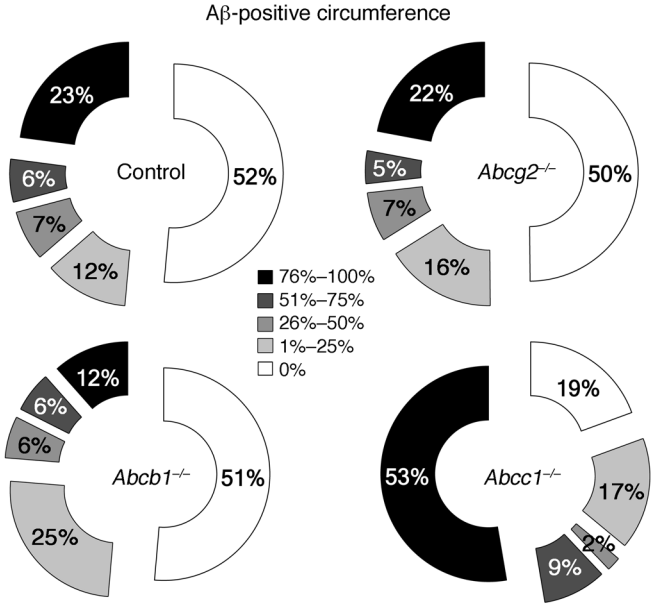

Figure 5
Aβ deposition is enhanced in the walls of brain microvessels in APP_{dt}×*Abcc1*$^{-/-}$ mice. The graphs present the proportion of meningeal vessel walls that were affected by different degrees of Aβ deposition (Aβ-positive circumference). Assessment of APP_{dt} mice deficient in ABCG2 or ABCB1, respectively, revealed no differences in CAA relative to APP_{dt} controls. In contrast, 53% of blood vessels were severely affected by CAA (>75% of the circumference is decorated with Aβ) in APP_{dt}×*Abcc1*$^{-/-}$ mice versus 23% in APP_{dt} controls. $n = 3$.

Discussion

We demonstrate for what we believe is the first time that the ATP-binding cassette transporter ABCC1 strongly influences cerebral Aβ accumulation in genetically modified mice. This finding, in conjunction with evidence that other ABC family transporters also convey Aβ (12, 13, 15, 16, 18), implicates this family of molecules in cerebral Aβ export impairments in AD patients (4). Our results identify ABCC1 in particular as a potential target for impeding the pathogenesis of Aβ proteopathies such as AD and CAA. Diminished ABCC1 function disrupts a salient route of Aβ clearance, leading to enhanced accumulation of the protein in the brain parenchyma and along the perivascular drainage channels that are important elimination pathways for Aβ (8, 26). Notably, ABCC1 also has been found to be highly expressed in cells of the choroid plexus (28, 29), which undergo significant functional and energetic changes during aging and AD (reviewed in ref. 30) that could diminish transport function in this structure.

How Aβ reaches its transporters at the luminal side of the brain barrier epithelia/ependyma is unknown, but the pronounced effects found in the present study indicate a bottleneck at the luminal rather than the abluminal membranes. One possible transcytotic mediator is LRP1, which can shuttle Aβ between the abluminal and luminal membranes, but the means by which LRP1 (or some as yet unidentified mediator) interacts functionally with the ABC transporters remains to be determined. ABC transporter dysfunction/dysregulation also has been implicated in Parkinson disease (PD), progressive supranuclear palsy (PSP), multisystem atrophy (MSA), and epilepsy (19, 31, 32). The induction of ABCC1 activity thus represents a promising strategy for treating or preventing AD and other neurodegenerative proteopathies. A number of approved pharmaceuticals and other substances interact with the ABC family of proteins in humans, and many of these agents inhibit ABC transporters (33). It will be important to determine whether chronic exposure to such agents influences the risk of developing certain neurodegenerative diseases.

Methods

Animals. *APP/PS1* and APP_{dt} mice were provided by M. Herzig, R. Radde, and M. Jucker (University of Tübingen, Tübingen, Germany) (22, 34). FVB.129P2-Abcg2^{tm1Ahs} N7 (*Abcg2*$^{-/-}$), FVB.129P2-Abcb1a^{tm1Bor} Abcb1b^{tm1Bor} N12 (*Abcb1*$^{-/-}$), and FVB.129P2-Abcc1a^{tm1Bor} N12 (*Abcc1*$^{-/-}$) mice were purchased from Taconic Farms (24, 35, 36). *APP/PS1* and APP_{dt} transgenic mice were crossed to transporter knockout mice for at least 9 generations into the FVB/N background for all strains. All mice were housed in a 12-hour light/12-hour dark cycle at 23°C with free access to food (SNIFF) and water.

Tissue preparation. For tissue preparation, mice were sacrificed by cervical dislocation and transcardially perfused with PBS. The brain was removed from each mouse, and one hemisphere was stored in buffered 4% PFA for paraffin embedding and immunohistochemistry, while the other hemisphere was snap-frozen in liquid nitrogen and stored at –80°C for biochemical analysis.

ELISA. ELISA kits (TH40HS, TK42HS: high sensitivity) from the Genetics Company were used for the quantification of Aβ40 and Aβ42 in whole brain hemispheres from which the cerebellum and brain stem had been removed at the level of the midbrain. Hemispheres were homogenized using a PreCellys24 (12 seconds, 6,500 rpm). After addition of carbonate buffer (pH 8.0), homogenates were mixed using the PreCellys (5 seconds, 5,000 rpm) and centrifuged for 90 minutes (4°C) at 24,000 *g* to separate insoluble from soluble Aβ species. The resulting supernatant (buffer-soluble fraction) was mixed with 8 M guanidine hydrochloride at a ratio of 1:1.6. To extract aggregated Aβ species, the pellet was dissolved in 8 volumes of 5 M guanidine hydrochloride, shaken at room temperature for 3 hours, and centrifuged at 24,000 *g* for 20 minutes at 4°C. The resulting supernatant represents the guanidine-soluble fraction. Protein contents of all samples were measured in triplicate using a NanoDrop 1000 (Thermo Fisher Scientific). ELISAs were performed according to the manufacturer's instructions using appropriate dilutions.

Expression analyses of APP and Aβ transporting/cleavage/degrading complex components. GeneChip Mouse Gene 1.0 Arrays interrogating more than 28,000 murine genes were used to investigate gene expression in *APP/PS1*×*Abcc1*$^{-/-}$ and *APP/PS1* mice. Array hybridization was performed according to the supplier's instructions using the Ambion WT Expression Kit (Ambion) plus the GeneChip WT Terminal Labeling and Hybridization Kit and the GeneChip Sample Cleanup Module (Affymetrix). For signal enhancement, an antibody amplification was carried out using a biotinylated antistreptavidin antibody (Vector Laboratories), which was cross-linked by goat IgG (Sigma-Aldrich) followed by a second staining with streptavidin-phycoerythrin conjugate (Molecular Probes; Invitrogen). The microarrays were scanned with the G7 upgraded GeneChip Scanner 3000 (Affymetrix) at 0.7 micron resolution. The data analysis was performed with the Partek Genomics Suite 6.5 software (Partek) using the Robust Multichip Analysis (RMA) algorithm, including an adjustment to the GC content (GCRMA), and employing the quantile normalization method. ANOVA was performed to statistically compare the candidate genes between the 2 groups (*APP/PS1* and

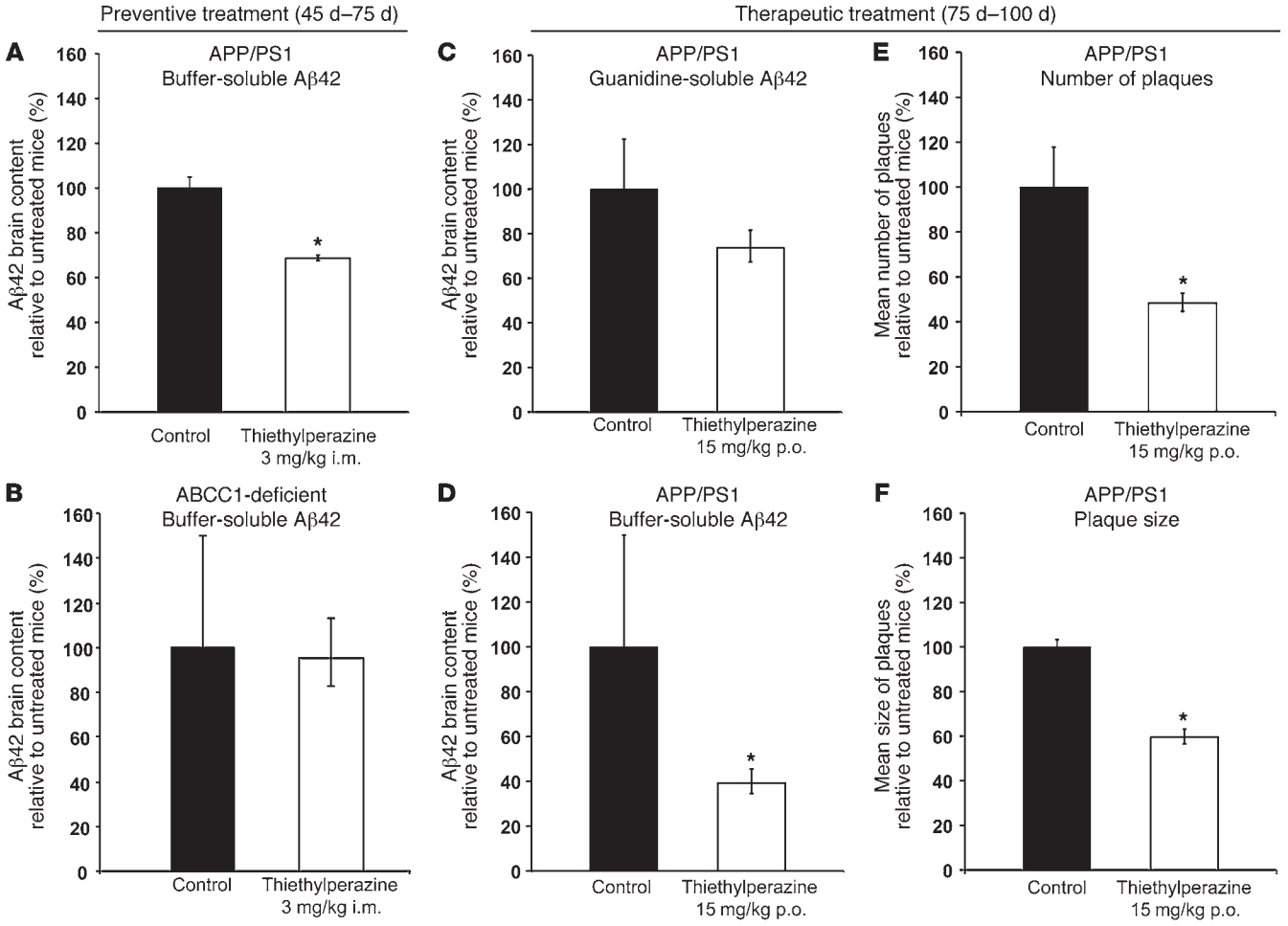

Figure 6
Activation of ABCC1 reduces Aβ levels. (**A** and **B**) Mice were treated i.m. with thiethylperazine twice daily for 30 days starting at 45 days of age. (**A**) Activation of ABCC1 by thiethylperazine reduces Aβ levels in *APP/PS1* mice. (**B**) The lack of an effect in treated *APP/PS1×Abcc1*$^{-/-}$ mice shows that Aβ reduction in *APP/PS1* mice is probably due to the induction of ABCC1. (**C**–**F**) Mice treated p.o. with 15 mg/kg thiethylperazine per day. Buffer-soluble Aβ (**D**) and plaque burden (**E** and **F**) are significantly reduced in treated *APP/PS1* mice. Error bars show SEM. $n \geq 4$. *$P < 0.05$.

APP/PS1×Abcc1$^{-/-}$) of 3 biological replicates each. The data have been deposited at the NCBI Gene Expression Omnibus (GEO GSE30762).

Western blots. For Western blotting, tissue homogenates were prepared as described by Lesné et al. (37). Total protein concentrations of the extracts were determined using a BCA assay (Pierce). After electrophoresis of 10 μg total protein per lane, proteins were blotted onto PVDF membranes. After blocking in 5% dry milk in TBST Buffer (50 mM Tris, pH 7.4, 150 mM NaCl, 0.1% Tween 20) for 1 hour at room temperature, blots were probed for either APP/Aβ (1:1,000, clone 6E10; Sigma-Aldrich), ADAM10 (1:1,000; Calbiochem), BACE1 (1:1,000; Abcam), IDE (1:500; Abcam), calreticulin (1:1,000; Cell Signaling), caspase-3 (1:1,000; Cell Signaling), COX-IV (1:1,000; Cell Signaling), or β-actin (1:20,000; Sigma-Aldrich) overnight at 4°C. As detection antibodies, anti–mouse-HRP, anti–rat-HRP and anti–rabbit-HRP, respectively, were used. The Amersham ECL Plus Detection Kit and a Roper CoolSnap HQ² Camera (Roper) were used for visualization.

Subcellular fractionation. Subcellular fractions of freshly isolated brains were prepared as described by Cox et al. (38) with slight modifications. Briefly, both hemispheres were dounce homogenized in IH buffer (250 mM saccharose; 10 mM Tris-HCl, pH 7.8; 0.3 mM PMSF; 0.2 mM EDTA; 1 μg/ml leupeptin; 1 μg/ml pepstatin) and centrifuged to pellet nuclei (1,000 *g*, 4°C, 10 minutes). The pellet was resuspended in IH buffer and rehomogenized by centrifuging through QIAShredder (QIAGEN) columns. Purification of nuclei was achieved via saccharose gradient centrifugation at 80,000 *g* for 40 minutes. Cytosolic, microsomal, and mitochondrial proteins were isolated by centrifugation of the initial supernatant (12,000 *g*, 4°C, 15 minutes). Mitochondria in the pellet were isolated using 2 cycles of washes with IH buffer and recentrifugation. The supernatant was centrifuged at 100,000 *g* for 60 minutes to pellet microsomes. The supernatant contained pure cytosolic proteins.

Immunohistochemistry. Formalin-fixed brains were embedded in paraffin and 4 μm–thick sections were cut. After deparaffinization, the sections were processed using the BOND-MAX Autostainer (Leica Microsystems GmbH/Menarini). Immunostaining was initiated after blocking endogenous peroxidase (5 minutes) and epitope retrieval for 5 minutes with 95% formic acid (for the 6F3D [Dako]), 70% formic acid (for antibody 4G8; Millipore) or 20 minutes with an EDTA buffer at pH 8.5 (for antibody Iba1, Wako; EDTA buffer was supplied by Leica Microsystems GmbH/Menarini).

Primary antibodies incubated routinely for 30 minutes at room temperature with dilutions were as follows: Dako clone 6F3D (1:100), 4G8 (1:500), and Iba1 (1:1,000). Primary antibodies were detected with the BOND-MAX Bond Polymer Refine Detection Kit and standard protocol DAB R30. Slides were fully digitized with a resolution of 230 nm using the Mirax Desk and Mirax Midi automated slide scanners, and then semiautomatically analyzed using the AxioVision software package (Zeiss) (23).

Assessment of CAA severity. Brain sections from APP_{dt} mice were stained using the 4G8 antibody. At least 2 nonconsecutive sections were inspected for CAA of meningeal vessels in a blinded fashion. All meningeal vessels were counted manually, and the severity of CAA was categorized as follows: category I, not affected; category II, ≤ 25% of circumference positively stained; category III, 26%–50% of circumference positively stained; category IV, 51%–75% of circumference positively stained; category V, 76%–100% of circumference positively stained (Supplemental Figure 8). The mean number of vessels belonging to each category was calculated relative to the overall number of vessels found.

ECTA. Mouse brain capillary endothelial cells were prepared as described by Coisne et al. (39). In brief, at least ten 3- to 4-week-old mice were decapitated and the brains removed. After dissecting the brain stem, white matter, and meninges, tissue was homogenized in 2 volumes of wash buffer B (WBB) (HBSS, 10 mM HEPES, 0.1% BSA) using a 15-ml glass douncer (Wheaton Industries). One volume of 30% dextran solution was added to the homogenate and centrifuged twice at 3,000 *g* at 4°C. The pellet containing the vessels was resuspended in WBB, and large vessels were ruptured manually by harsh pipetting of the solution. Vacuum filtration through a 60-μm membrane (SEFAR) was used to separate large vessels from capillaries. After combined collagenase/dispase (HBSS, 10 mM HEPES, 0.15 μg/ml TCLK, 10 μg/ml DNAse-I, 1 mg/ml collagenase/dispase [Roche]) treatment, single-cell suspension was achieved by another harsh pipetting of the solution. Endothelial cells were seeded into Matrigel-coated Transwell inserts (0.4 μm pores, Greiner Bio-One) with a density of 120,000 cells per insert and grown on top of a supportive glial culture. P_e calculation according to ref. 40 using Lucifer yellow was used to determine paracellular flow during the assays. In brief, the average volume cleared was plotted versus time and the slope was estimated by linear regression analysis. PS is the permeability surface area product (in ml/min), and the calculated slope corresponds to the P_{St}. The slope of the clearance curve with the control insert (filter coated with Matrigel without cells) was denoted P_{Sf}. The P_S value for the EC monolayer (P_{Se}) was calculated as follows: $1/P_{Se}=1/P_{St}-1/P_{Sf}$. The P_{Se} value was then divided by the surface area of the filters (A_O = 1.13 cm^2) to generate the endothelial permeability (P_e, in cm/min). Inserts with a P_e higher than 1.6×10^{-3} cm/min were discarded for Aβ transport analyses. Active Aβ42 transport was calculated as $C_{A\beta} \times V_{lc} \times (1-(C_{Lm}/C_{Li}))$ to control for paracellular flow, where $C_{A\beta}$ and V_{lc} refer to the Aβ42 concentration measured and the volume of the luminal chamber, respectively. C_{Lm} corresponds to the amount of Lucifer yellow that passed the Transwell monolayer, and C_{Li} as the initial amount of Lucifer yellow. For Aβ transport studies, culture medium from the abluminal compartment was replaced with solution containing 10 ng Aβ42 (1.6 nM final concentration). Subsequently, the samples were taken from the luminal compartment after 0.5, 1, 2, 6, and 24 hours. Aβ content was determined by ELISA.

ABCC1 activity assay. In vitro ABCC1 activity was measured using the SB MRP1 PREDEASY ATPase Kit (Solvo Biotechnology) according to the manufacturer's instructions. In brief, a provided membrane preparation of Sf9 cells containing human ABCC1 was diluted in assay buffer to provide 8 μg membrane per well. Assay mixtures were prepared either with or without NEM-GS as standard substrate and with or without vanadate to control for nonspecific ATPase activities. Thiethylperazine was diluted in DMSO (Sigma-Aldrich) and added to the appropriate wells (final concentration 1.3 ng/ml). Pipetting was done strictly on ice. After addition of thiethylperazine, the 96-well plate was incubated at 37°C for 10 minutes. The reaction was started by adding 10 μl of 10 mM MgATP. After 10 minutes of incubation at 37°C, the reaction was stopped by adding 100 μl developer. Two minutes later, 100 μl blocking solution was added. The reaction mix was then incubated for a further 30 minutes at 37°C. Finally, 96-well plates were measured using a Paradigm spectrophotometer (Beckman-Coulter) at 610 nm.

Statistics. The Lilliefors goodness-of-fit test ($\alpha = 0.05$) was applied to the ELISA data and to the log-transformed ELISA data to distinguish between the assumption of normally distributed sample data and the assumption of log-normally distributed sample data. Despite the small sample size, for both data sets, the null hypothesis was rejected for 5 out of 44 samples (Supplemental Table 4). Consistent with the observation of predominantly positive skew and strict positive sample data, the assumption of normally distributed data was discarded. Mean values and confidence intervals were calculated assuming an underlying log-normal distribution. The Wilcoxon rank-sum test was applied to compare all data from the different mouse strains for each time point (for resulting *P* values of ELISA measurements, see Supplemental Table 4). $P \leq 0.05$ was considered significant.

Study approval. The experiments were designed to minimize the number of animals used and were approved by local authorities: Landesamt für Landwirtschaft, Lebensmittelsicherheit und Fischereiwesen (LALLF) (LALLF M-V/TSD/7221.3-2.3-004/06, LALLF M-V/TSD/7221.3-2.3-003/08, LALLF M-V/TSD/7221.3-1.1-004/11.

Acknowledgments

The authors thank D. Koczan, O. Wolkenhauer, and R. Benecke for their support and discussion. This work was supported by grants from the Alzheimer Forschung Initiative e.V. (no. 09857 to J. Pahnke), BMBF: German Ministry for Education and Research (FORSYS no. 0315255 to K. Rateitschak), the NIH (RR-00165) (to L.C. Walker), the University of Rostock Interdisciplinary Faculty (to. M. Krohn and F. Winter), and the Excellence Initiative Mecklenburg-Vorpommern (to J. Pahnke).

Received for publication March 4, 2011, and accepted in revised form July 20, 2011.

Address correspondence to: Jens Pahnke, University of Rostock, Neurodegeneration Research Laboratory (NRL), Gehlsheimer Str. 20, 18147 Rostock, Germany. Phone: 49.381.494.4700; Fax: 49.381.494.4702; E-mail: jens.pahnke@googlemail.com.

1. Balch WE, Morimoto RI, Dillin A, Kelly JW. Adapting proteostasis for disease intervention. *Science*. 2008;319(5865):916–919.
2. Selkoe DJ. Clearing the brain's amyloid cobwebs. *Neuron*. 2001;32(2):177–180.
3. Querfurth HW, LaFerla FM. Alzheimer's disease. *N Engl J Med*. 2010;362(4):329–344.
4. Mawuenyega KG, et al. Decreased clearance of CNS beta-amyloid in Alzheimer's disease. *Science*. 2010;330(6012):1774.
5. Wong E, Cuervo AM. Autophagy gone awry in neurodegenerative diseases. *Nat Neurosci*. 2010;13(7):805–811.
6. Lipinski MM, et al. Genome-wide analysis reveals mechanisms modulating autophagy in normal brain aging and in Alzheimer's disease. *Proc Natl Acad Sci U S A*. 2010;107(32):14164–14169.
7. Deane R, et al. RAGE mediates amyloid-beta peptide transport across the blood-brain barrier and accumulation in brain. *Nat Med*. 2003;9(7):907–913.
8. Weller RO, Subash M, Preston SD, Mazanti I, Carare RO. Perivascular drainage of amyloid-beta peptides from the brain and its failure in cerebral amyloid angiopathy and Alzheimer's disease. *Brain Pathol*. 2008;18(2):253–266.
9. Pahnke J, Walker LC, Scheffler K, Krohn M. Alzheimer's disease and blood-brain barrier func-

tion-Why have anti-beta-amyloid therapies failed to prevent dementia progression? *Neurosci Biobehav Rev*. 2009;33(7):1099–1108.
10. Deane R, Wu Z, Zlokovic BV. RAGE (yin) versus LRP (yang) balance regulates alzheimer amyloid beta-peptide clearance through transport across the blood-brain barrier. *Stroke*. 2004; 35(11 suppl 1):2628–2631.
11. Shibata M, et al. Clearance of Alzheimer's amyloid-ss(1-40) peptide from brain by LDL receptor-related protein-1 at the blood-brain barrier. *J Clin Invest*. 2000;106(12):1489–1499.
12. Kuhnke D, et al. MDR1-P-Glycoprotein (ABCB1) mediates transport of Alzheimer's amyloid-beta peptides--implications for the mechanisms of Abeta clearance at the blood-brain barrier. *Brain Pathol*. 2007;17(4):347–353.
13. Lam FC, et al. beta-Amyloid efflux mediated by p-glycoprotein. *J Neurochem*. 2001;76(4):1121–1128.
14. Hartz AM, Miller DS, Bauer B. Restoring blood-brain barrier P-glycoprotein reduces brain amyloid-beta in a mouse model of Alzheimer's disease. *Mol Pharmacol*. 2010;77(5):715–723.
15. Vogelgesang S, et al. The role of P-glycoprotein in cerebral amyloid angiopathy; implications for the early pathogenesis of Alzheimer's disease. *Curr Alzheimer Res*. 2004;1(2):121–125.
16. Xiong H, et al. ABCG2 is upregulated in Alzheimer's brain with cerebral amyloid angiopathy and may act as a gatekeeper at the blood-brain barrier for Abeta (1-40) peptides. *J Neurosci*. 2009;29(17):5463–5475.
17. Cirrito JR, et al. P-glycoprotein deficiency at the blood-brain barrier increases amyloid-beta deposition in an Alzheimer disease mouse model. *J Clin Invest*. 2005;115(11):3285–3290.
18. Koldamova R, Staufenbiel M, Lefterov I. Lack of ABCA1 considerably decreases brain ApoE level and increases amyloid deposition in APP23 mice. *J Biol Chem*. 2005;280(52):43224–43235.
19. Pahnke J, Wolkenhauer O, Krohn M, Walker LC. Clinico-pathologic function of cerebral ABC transporters - implications for the pathogenesis of Alzheimer's disease. *Curr Alzheimer Res*. 2008;5(4):396–405.
20. Sharom FJ. ABC multidrug transporters: structure, function and role in chemoresistance. *Pharmacogenomics*. 2008;9(1):105–127.
21. Burgold S, et al. In vivo multiphoton imaging reveals gradual growth of newborn amyloid plaques over weeks. *Acta Neuropathol*. 2011;121(3):327–335.
22. Radde R, et al. Abeta42-driven cerebral amyloidosis in transgenic mice reveals early and robust pathology. *EMBO Rep*. 2006;7(9):940–946.
23. Scheffler K, et al. Determination of spatial and temporal distribution of microglia by 230nm-high-resolution, high-throughput automated analysis reveals different amyloid plaque populations in an APP/PS1 mouse model of Alzheimer's disease [published online ahead of print January 19, 2011]. *Curr Alzheimer Res*. PMID: 21244350.
24. Wijnholds J, et al. Increased sensitivity to anticancer drugs and decreased inflammatory response in mice lacking the multidrug resistance-associated protein. *Nat Med*. 1997;3(11):1275–1279.
25. Levy E, Prelli F, Frangione B. Studies on the first described Alzheimer's disease amyloid beta mutant, the Dutch variant. *J Alzheimers Dis*. 2006; 9(3 suppl):329–339.
26. Monro OR, et al. Substitution at codon 22 reduces clearance of Alzheimer's amyloid-beta peptide from the cerebrospinal fluid and prevents its transport from the central nervous system into blood. *Neurobiol Aging*. 2002;23(3):405–412.
27. Wesołowska O, Molnar J, Ocsovszki I, Michalak K. Differential effect of phenothiazines on MRP1 and P-glycoprotein activity. *In Vivo*. 2009;23(6):943–947.
28. Rao VV, et al. Choroid plexus epithelial expression of MDR1 P glycoprotein and multidrug resistance-associated protein contribute to the blood-cerebrospinal-fluid drug-permeability barrier. *Proc Natl Acad Sci U S A*. 1999;96(7):3900–3905.
29. Wijnholds J, et al. Multidrug resistance protein 1 protects the choroid plexus epithelium and contributes to the blood-cerebrospinal fluid barrier. *J Clin Invest*. 2000;105(3):279–285.
30. Serot JM, Bene MC, Faure GC. Choroid plexus, aging of the brain, and Alzheimer's disease. *Front Biosci*. 2003;8:s515–s521.
31. Bartels AL, van Berckel BN, Lubberink M, Luurtsema G, Lammertsma AA, Leenders KL. Blood-brain barrier P-glycoprotein function is not impaired in early Parkinson's disease. *Parkinsonism Relat Disord*. 2008;14(6):505–508.
32. Volk HA, Burkhardt K, Potschka H, Chen J, Becker A, Loscher W. Neuronal expression of the drug efflux transporter P-glycoprotein in the rat hippocampus after limbic seizures. *NeuroScience*. 2004;123(3):751–759.
33. Lee CH. Reversing agents for ATP-binding cassette drug transporters. *Methods Mol Biol*. 2010; 596:325–340.
34. Herzig MC, et al. Abeta is targeted to the vasculature in a mouse model of hereditary cerebral hemorrhage with amyloidosis. *Nat Neurosci*. 2004;7(9):954–960.
35. Jonker JW, et al. The breast cancer resistance protein protects against a major chlorophyll-derived dietary phototoxin and protoporphyria. *Proc Natl Acad Sci U S A*. 2002;99(24):15649–15654.
36. Schinkel AH, et al. Disruption of the mouse mdr1a P-glycoprotein gene leads to a deficiency in the blood-brain barrier and to increased sensitivity to drugs. *Cell*. 1994;77(4):491–502.
37. Lesné S, et al. A specific amyloid-beta protein assembly in the brain impairs memory. *Nature*. 2006;440(7082):352–357.
38. Cox B, Emili A. Tissue subcellular fractionation and protein extraction for use in mass-spectrometry-based proteomics. *Nat Protoc*. 2006;1(4):1872–1878.
39. Coisne C, et al. Mouse syngenic in vitro blood-brain barrier model: a new tool to examine inflammatory events in cerebral endothelium. *Lab Invest*. 2005;85(6):734–746.
40. Siflinger-Birnboim A, Cooper JA, del Vecchio PJ, Lum H, Malik AB. Selectivity of the endothelial monolayer: effects of increased permeability. *Microvasc Res*. 1988;36(3):216–227.